# Late Miocene-Pliocene climate evolution recorded by the red clay covered on the Xiaoshuizi planation surface, NE Tibetan Plateau

Xiaomiao Li[1], Tingjiang Peng[1], Zhenhua Ma[1], Meng Li[1], Zhantao Feng[1], Benhong Guo[1], Hao Yu[1], Xiyan Ye[1], Zhengchuang Hui[1], Chunhui Song[2], Jijun Li[1, 3]

1. MOE Key Laboratory of Western China's Environmental Systems, College of Earth and Environmental Sciences, Lanzhou University, Lanzhou 730000, China

2. School of Earth Sciences, Key Laboratory of Western China's Mineral Resources of Gansu Province, Lanzhou University, Lanzhou 730000, China

3. College of Geography Science, Nanjing Normal University, Nanjing 210023, China

*Corresponding author: Key Laboratory of Western China's Environmental Systems (Ministry of Education), College of Earth and Environmental Science, Lanzhou University, Lanzhou 730000, China; *E-mail address*: lijj@lzu.edu.cn (J.J. Li), *Fax*: +86-931-891-2724; *Tel.:* +86-931-891-2724

**Abstract**

The Pliocene climate and its driving mechanisms have attracted substantial scientific interest because of their potential as an analog for near-future climates. The late Miocene-Pliocene red clay sequence of the main Chinese Loess Plateau (CLP) has been widely used to reconstruct the history of interior Asian aridification and the Asian monsoon. However, red clay sequences deposited on the planation surface of the Tibetan Plateau (TP) are rare. A continuous red clay sequence was recently discovered on the uplifted Xiaoshuizi (XSZ) planation surface in the Maxian Mountains, northeastern (NE) TP. In this study, we analyzed multiple climatic proxies from the XSZ red clay sequence with the aim of reconstructing the late Miocene-early Pliocene climate history of the NE TP and to assess regional climatic differences between the central and western CLP. Our results demonstrate the occurrence of minimal weathering and pedogenesis during the late Miocene, which indicates that the climate was arid. We speculate that precipitation delivered by the palaeo- East Asian Summer Monsoon (EASM) was limited during this period, and that the intensification of the westerlies circulation resulted in arid conditions in the study region. Subsequently, enhanced weathering and pedogenesis occurred intermittently during 4.7-3.9 Ma, which attests to an increase in effective moisture. We ascribe the arid-humid climatic transition near ~4.7 Ma to the expansion of the palaeo-EASM. The warming of the high northern latitudes in response to the closure of the Panamanian seaway, may have been responsible for the thermodynamical enhancement of the palaeo-EASM system, which permitted more moisture to be transported to the NE TP.

**Keywords:** Late Miocene-Pliocene; Xiaoshuizi Planation Surface; Red Clay; Palaeo-EASM;

45 Westerly Circulation

46

47 **1. Introduction**

48 The Pliocene, including the Zanclean (5.33-3.60 Ma) and Piacenzian (3.60-2.58 Ma)
49 stages, is one of the most intensively studied intervals of the pre-Quaternary in climate
50 change research. The Zanclean climate was generally warm and wet and is often used as an
51 analogue for near-future climate conditions in terms of carbon dioxide levels, ranging from
52 280-415 ppm (Tripati et al., 2009; Pagani et al., 2010), and comparable temperatures in the
53 tropical region (Herbert et al., 2010, 2016). On the other hand, the Zanclean was markedly
54 different from today, although several critical changes in thermohaline and atmospheric
55 circulation towards modern conditions were occurring (Haug et al., 2005; Lawrence et al.,
56 2006; Chaisson and Ravelo, 2000). For example, the early-Pliocene global mean
57 temperature was approximately 4 ℃ warmer (Brierley and Fedorov, 2010), and the sea
58 levels are estimated to have been ~25 m higher, than today (Dowsett et al., 2010).
59 Temperatures at high northern latitudes were considerably higher and therefore continental
60 glaciers were almost absent from the Northern Hemisphere (Ballantyne et al., 2010; Dowsett
61 et al., 2010). The zonal and meridional sea surface temperature gradients in the Northern
62 Hemisphere were weak but gradually became more intensified, changing towards the
63 modern state which has a much more pronounced spatial temperature contrast (Fedorov et
64 al., 2013; Brierley et al., 2009, 2010). The low meridional surface temperature gradient
65 resulted in weaker meridional circulation during this interval ( Fedorov et al., 2013; Brierley

et al., 2009), and the minor east-west sea surface temperature contrast in the tropical Pacific during this interval is believed to have given rise to a permanent El Nino Southern Oscillation (Lawrence et al., 2006); however, whether permanent El Nino–like conditions were sustained during the Pliocene is controversial (Wara et al., 2005; Watanabe et al., 2011; Zhang et al., 2014). In addition, the episodic uplift of the TP (Li et al., 2015; Zheng et al., 2000; Fang et al., 2005a, 2005b) and gradual closure of the Panama Seaway (Keigwin et al., 1978; O'Dea et al., 2016) were underway. The former had a substantial climatic impact (An et al., 2001; Ding et al., 2001; Liu et al., 2014) and the latter resulted in the reorganization of the global thermohaline circulation system (Haug et al., 1998, 2001). These features imply a spatial change in the organization of the global climate system from the early Pliocene to the present. In this context, it is important to characterize the response of regional climates to these major global climatic and tectonic changes.

East Asia is one of the key regions for studying the aridification of the Asian interior and the Asian monsoon evolution, which are tightly linked to the uplift of the TP, regional climate change, and the evolution of global temperature and ice volume (An et al., 2001; Ding et al., 2001; Li et al., 2008; Clift et al., 2008; Nie et al., 2014; Ao et al., 2016; Sun et al., 2006a, 2017; Chang et al., 2013; Liu et al., 2014). Previous research has revealed that red clay was widely deposited across the CLP since the late Miocene, indicating that Asian aridification was enhanced (Guo et al., 2001; Song et al., 2007; An et al., 2014; Ao et al., 2016; Li et al., 2017). In the eastern and central CLP, where the climate is dominated by the East Asian Monsoon, palaeontological evidence, mineral magnetic parameters and geochemical records from the red clay indicate dry climatic conditions during the late

Miocene but generally wet climatic conditions during the early Pliocene (Wang et al., 2006; Guo et al., 2001; Wu et al., 2006; Song et al., 2007; Sun et al., 2010; An et al., 2014; Ao et al., 2016). The most controversial climatic change occurred during the interval from 4.8-4.1 Ma, for which climate reconstructions using different proxies indicate conflicting palaeo-environmental trends. For example, field observations and pollen records indicate an intensified summer monsoon intensity, but low magnetic susceptibility values are more consistent with arid rather than wet climatic conditions (Ding et al., 2001; Ma et al., 2005; Song et al., 2007; Sun et al., 2010). It is thought that dissolution of ferrimagnetic minerals and iron reduction resulting from high precipitation significantly affected the climatic significance of magnetic susceptibility records during this period (Ding et al., 2001). In addition to the East Asian Monsoon, the westerlies also had an impact on the climate of East Asia; however, the patterns of climate change in the westerlies-dominated regions were different from the eastern and central CLP during the early Pliocene. Geochemical, stratigraphic and pollen evidence from the Qaidam and Tarim basins has demonstrated that aridification intensified since the early Pliocene (Fang et al., 2008; Sun et al., 2006a, 2017; Chang et al., 2013; Liu et al., 2014). Although the general climatic trends of the main CLP and central Asia during this period are well recorded, palaeoclimatic changes in the NE TP, which is at the junction of the zones of westerlies and monsoonal influences, remain unclear. Therefore, determining the climatic conditions of the NE TP during the early Pliocene not only improves our understanding of the pattern of regional climate change, but it may also provide insights into the responses of the palaeo-EASM and the westerlies to TP uplift and changes in the global climate system.

A continuous red clay sequence was recently discovered on the uplifted XSZ planation surface in the NE TP and has been dated via high-resolution magnetostratigraphy (Li et al., 2017). Due to its specific geographical location, the XSZ red clay provides the opportunity to reveal the late Miocene-early Pliocene climate history of the NE TP and to determine the climatic differences between the central and western CLP. In this study, we measured multiple climatic proxies from the late Miocene-Pliocene XSZ red clay core. Our aims were to construct a detailed record of precipitation, chemical weathering and pedogenesis during 6.7-3.6 Ma; and to determine the pattern of regional climate evolution and its possible causal mechanisms.

## 2. Regional background

The XSZ planation surface is located in Yuzhong County in the western Chinese Loess Plateau (Fig. 1). The main XSZ planation surface is at an altitude of 2800 m in the Maxian Mountains where it has truncated Precambrian gneiss. The Maxianshan are rejuvenated mountains which protrude into the broad Longzhong Basin; they are located within a climatically sensitive zone because of the combined influences of the Asian Monsoon and the northern branch of the mid-latitude westerly circulation system. The planation surface is mantled by over 30 m of loess and over 40 m of red clay. Our previous bio-magnetostratigraphic study demonstrates that the red clay sequence covering the XSZ planation surface is dated to ~6.9-3.6 Ma (Li et al., 2017). Here, we use the XSZ drill core to reconstruct and discuss the patterns of regional climate change during the Miocene-Pliocene. The long, continuous well-dated record of the drill core is superior to that of the Shangyaotan

core analyzed in Li et al. (2017). Yuzhong County lies within the semi-arid temperate climate zone at the junction of the eastern monsoon area, the arid area of northwest China, and the cold region of the TP. The mean annual temperature during 1986-2016 was ~7.0 ℃ and the annual precipitation was 260-550 mm; 80% of the precipitation is in summer and autumn (data source: National Meteorological Information Center (http://data.cma.cn/) of the Chinese Meteorological Administration). The spatial distribution of precipitation is uneven, decreasing from south to north in Yuzhong County. Precipitation amount increases with elevation at the rate of 27 mm per 100 m, attaining a maximum of 800 mm at the top of Maxianshan.

## 3. Material and methods

The XSZ core (35.8115 ℃N, 103.8623 ℃E and 2758.1 m above sea level) is composed of 42 m of pure red clay and ~3 m of red clay and there is an increasing content of angular gravel at the base (Fig. 1 b). The red clay interval is composed of brownish red and yellowish clay layers (Fig. 2). The upper 20 m contains numerous horizontal carbonate nodule horizons (Bk), most of which underlie brownish red soil layers (Bw) characterized by loam and moderate medium angular blocky structure. There are also occasional carbonized plant root channels, elliptical worm burrows and fossil snail shell fragments. Fe-Mn stains are more frequent in the brownish layers than in the yellowish layers, which is also the case for the carbonized root channels. The red clay across the XSZ planation surface is similar to that of typical eolian red clay in the CLP; both are characterized by numerous carbonate nodule-rich horizons (Fig. 2 b).

Samples for grain-size, carbonate content and magnetic susceptibility measurements were taken at 5-cm intervals, and samples for geochemical analysis were collected at 25-cm intervals. Samples for grain-size measurements were pre-treated with 10% $H_2O_2$ to remove organic material, with 10% HCl to remove carbonates, and with 0.05 mol/L of $(NaPO_3)_6$ for dispersion. They were then measured with a Malvern Mastersizer 2000 grain-size analyzer with a detection range of 0.02-2000 μm. Magnetic susceptibility was measured using a Bartington Instruments MS2 meter and MS2B dual-frequency sensor at two frequencies (470 Hz and 4700 Hz, designated $\chi_{lf}$ and $\chi_{hf}$, respectively). Three measurements were made at each frequency and the final results were averaged. The frequency-dependent magnetic susceptibility ($\chi_{fd}$) was calculated as $\chi_{lf}-\chi_{hf}$. Chemical composition was measured via X-ray fluorescence using a Panalytical Magix PW2403 with an error of 0.1%-0.3%. The sample preparation procedure for XRF analysis was as follows: Bulk samples were heated to 35℃ for 7 days and then ground with an agate mortar to pass a 75-μm sieve; ~4 g of powdered sample was then pressed into a pellet with a borate coating using a semiautomatic oil-hydraulic laboratory press (model YYJ-40). All the measurements were conducted at the MOE Key Laboratory of Western China's Environmental Systems, Lanzhou University. Silicate-bound CaO (CaO*) can be estimated, in principle, by the equation: CaO*(mol) = CaO(mol) – $CO_2$(calcite mol) − 0.5 $CO_2$(dolomite mol) − 10/3 $P_2O_5$(apatite mol) (Fedo et al., 1995). It is generally calculated based on the assumption that all the $P_2O_5$ is associated with apatite and all the inorganic carbon is associated with carbonates. Thus, the CaO* of the XSZ red clay was calculated using the following equivalent equation:

$$CaO^*(mol) = CaO(mol) - CaCO_3(mol) - \frac{10}{3} * \frac{P_2O_5}{M(P_2O_5)}$$

176 The carbonate content was measured with a calcimeter using the volumetric method of
177 Avery and Bascomb (1974) in the Key Laboratory of Mineral Resources in Western China
178 (Gansu Province), Lanzhou University.

179 We used the coefficient of variation (CV) to measure the variability of the records: the
180 higher the CV, the more variable the record. The CV is defined as:

$$CV=100*\frac{Standard\ deviation}{Mean}$$

181 Each sample age was estimated using linear interpolation to derive absolute ages,
182 constrained by our previous magnetostratigraphic study (Fig. 1). The average temporal
183 resolution of the records is 3.8 kyr. Some 80 % of the sequence has a sampling resolution of 4
184 kyr or less. After interpolation to a 3-kyr sampling interval, we performed spectral analysis
185 on detrended records of carbonate content and $\chi_{pedo}$ using Redfit, based on the Lomb-Scargle
186 Fourier transform combined with a Welch-Overlapped Segment averaging procedure. We
187 applied Gaussian band-pass filters at frequencies of 0.09090-0.01111, 0.02174-0.02778 and
188 0.04167-0.05556 $kyr^{-1}$ to extract oscillations associated with the 100-kyr, 41-kyr and 21-kyr
189 periodicities, respectively. The significance of the correlations is based on a two-tailed test.

190 **4. Results**

191 Profiles of the various environmental proxies are illustrated in Figure 3. Notably, there is
192 evidence for a relatively wet interval from ~16-5 m (4.7-3.9 Ma) which is reflected in the
193 high-frequency occurrence of Bw horizons with a low carbonate content (< 8%) and
194 intermittent enhancement of magnetic susceptibility. There is a large contrast in carbonate
195 content between Bw and Bk horizons, which corresponds to variations in elemental contents.
196 The Bk horizons, with a higher carbonate content, consist of carbonate nodule layers

underlying leached zones in the field indicate the substantial translocation of carbonate minerals from Bw horizons to Bk horizons due to greater rainfall (He et al., 2013). In addition, the CV of most of the records is greater during this interval than in other intervals (Table 1). These various forms of evidence suggest that the climate became more humid and variable during 4.7-3.9 Ma. The characteristics of the individual proxy records are described in detail below.

**Carbonate content**

The carbonate content of the entire core fluctuates from 1.6-39.2% with an average of 15.9 %. From 42-16 m, the average carbonate content is high (17.1%) and the carbonate content decreases upwards. The contrast in the carbonate content between the Bw and Bk horizons is generally low; for the Bw horizons, the carbonate content is ~12% and values <8% are rare. Bk horizons, with a carbonate content of around or above 21%, are frequent (Fig. 3). From 16-5 m, there are fluctuations in carbonate content of large amplitude (1.6-39.1%) but the average value is low (13.3%). Bw-Bk horizons are frequent; the Bw horizons have a carbonate content of <8%, while that of the Bk horizons is >21%. From 5-0 m, the average carbonate content increases to 15.5%; Bw horizons with a carbonate content <8% is absent, and the carbonate content contrast between the Bw and Bk horizons is low.

**Element geochemistry**

$K_2O$ ranges from 1.9-3.7% with an average of 2.8%; $Na_2O$ ranges from 0.14-1.54% with an average of 1.2%; Rb ranges from 74-134 ppm with an average of 106.2 ppm; and Sr ranges from 141-281 ppm with an average of 212.8 ppm. The variations in CaO exhibit the same trend as carbonate content with high values in Bk horizons and low values in Bw

horizons. The variations in Rb and $K_2O$ are synchronous and roughly inverse to those of CaO. The changes of Sr show some similarity with magnetic susceptibility prior to 4.7 Ma but with CaO after 4.7 Ma. Reference to Table 2 shows that CaO is positively correlated with $CaCO_3$ and Sr, and negatively correlated with the other elements. From 16-5 m, CaO and Sr exhibit low values in Bw horizons and high values in Bk horizons, while the opposite is the case for $K_2O$ and Rb. Finally, from 16-5 m, the amplitudes of the fluctuations in CaO, $K_2O$, Sr and Rb are greater than in the other intervals.

**Magnetic susceptibility**

The variations of $\chi_{hf}$, $\chi_{lf}$ and $\chi_{fd}$ are synchronous. $\chi_{hf}$ ranges from 9.6-53.9$\times10^{-8}$ $m^3$/kg with an average of 21.8$\times10^{-8}$$m^3$/kg; $\chi_{lf}$ ranges from 11.4-59.0$\times10^{-8}$ $m^3$/kg with an average of 23.1$\times10^{-8}$ $m^3$/kg; and $\chi_{fd}$ ranges from 0-4.7$\times10^{-8}$ $m^3$/kg with an average of 1.2$\times10^{-8}$ $m^3$/kg. From 42-16 m, the three magnetic parameters are relatively low and uniform. $\chi_{hf}$ ranges from 9.6-33.3$\times10^{-8}$ $m^3$/kg with an average of 19.4$\times10^{-8}$$m^3$/kg; $\chi_{lf}$ ranges from 11.4-36.1$\times10^{-8}$ $m^3$/kg with an average of 20.3$\times10^{-8}$ $m^3$/kg; and $\chi_{fd}$ ranges from 0-2.8$\times10^{-8}$ $m^3$/kg with an average of 1.0$\times10^{-8}$ $m^3$/kg. From 16-5 m, the values of the three parameters, together with their amplitudes of variation, are high. $\chi_{hf}$ ranges from 13.8-53.9$\times10^{-8}$ $m^3$/kg with an average of 27.4$\times10^{-8}$ $m^3$/kg; $\chi_{lf}$ ranges from 14.2-59.0$\times10^{-8}$ $m^3$/kg with an average of 29.0$\times10^{-8}$ $m^3$/kg; and $\chi_{fd}$ ranges from 0-4.7$\times10^{-8}$ $m^3$/kg with an average of 1.6$\times10^{-8}$ $m^3$/kg. Within the intervals of 16-15 m, 13-11 m and 7-5 m, the values of the three parameters increase substantially. From 5-0 m, both the values and amplitudes of variation of the three parameters decrease. $\chi_{hf}$ ranges from 12.8-32.9$\times10^{-8}$ $m^3$/kg with an average of 22.0$\times10^{-8}$ $m^3$/kg; $\chi_{lf}$ ranges from 13.6-34.6$\times10^{-8}$ $m^3$/kg with an average of 22.9$\times10^{-8}$ $m^3$/kg; and $\chi_{fd}$ ranges from 0-2.5$\times10^{-8}$ $m^3$/kg

with an average of $1 \times 10^{-8}$ $m^3$/kg. Overall, the fluctuations in magnetic susceptibility are substantially different to those of carbonate content which indicates that the enhancement of magnetic susceptibility was not caused by carbonate leaching.

**Grain size**

The clay content (<2 μm) ranges from 3.8-13.5% with an average of 8.17%; and the >40 um content ranges from 0.7-13.9% with an average of 6%. The fluctuations in clay content are minor, except for maxima at about 15 m, 12 m and 6 m, which correspond to peaks in magnetic susceptibility (Fig. 3). The coarse silt component (>40 μm), mainly carried by the East Asian winter monsoon, exhibits a different trend to that of the clay content. In addition, from 21-5 m the fluctuations in the >40 um fraction are roughly the inverse to those of magnetic susceptibility. From 42-21 m, the variation of the >40 μm fraction is characterized by low values and high-frequency fluctuations, whereas above 21 m it exhibits high values and fluctuations of lower frequency.

## 5. Discussion

### 5.1 Palaeoenvironmental interpretation of the proxies

The carbonate content of aeolian sediments can be readily remobilized and deposited in responses to changes in precipitation and evaporation intensity and thus is sensitive to changing climatic conditions. Previous studies demonstrated that the carbonate content of loess-red clay sequences of the CLP varies with precipitation (Fang et al., 1999; Sun et al., 2010). The carbonate is mainly derived from a mixture of airborne dusts (Fang et al., 1999). Soil micromorphological evidence from the Lanzhou loess demonstrates that the carbonate

grains in loess are little altered, whereas those in the palaeosols have undergone a reduction in size as a result of leaching and reprecipitation as secondary carbonate in the lower Bk horizons (Fang et al., 1994, 1999). Furthermore, seasonal alternations between wet and dry conditions are thought to be a key factor driving carbonate dissolution and reprecipitation (Sun et al., 2010). Thus, changes in carbonate content are generally controlled by the effective precipitation. When effective precipitation is high, carbonate leaching increases, and vice versa. Thus, the carbonate content is an effective proxy for characterizing wet-dry oscillations as well as summer monsoon evolution (Fang et al., 1999; Sun et al., 2010).

Chemical weathering intensity is generally evaluated by the ratio of mobile (e.g. K, Ca, Sr and Na) to non-mobile elements (e.g. Al and Rb). In general, Sr shows analogous geochemical behavior to Ca and is readily released into solution and mobilized in the course of weathering; by contrast, Rb is relatively immobile under moderate weathering conditions due to its strong adsorption to clay minerals (Nesbitt et al., 1980; Liu et al., 1993). Thus, the Rb/Sr ratio potentially reflects chemical weathering intensity. However, Sr may substitute for Ca in carbonates which may limit the environmental significance of the Rb/Sr ratio (Chang et al., 2013; Buggle et al., 2011). The correlation between Sr and CaO* (silicate CaO) is significant at the 99% confidence interval, while the correlation between Sr and $CaCO_3$ is not significant. This means that the variations in Sr are determined by weathering intensity, and therefore we speculate that in our samples the Rb/Sr ratio mainly reflects weathering intensity (Fig. 4 c and d). In addition, the $K_2O/Na_2O$ ratio is used to evaluate the secondary clay content in loess and is also a measure of plagioclase weathering, avoiding biases due to uncertainties in separating carbonate Ca from silicate Ca (Liu et al., 1993; Buggle et al.,

2011). $Na_2O$ is mainly produced by plagioclase weathering and is easily lost during leaching as precipitation increases. By contrast, $K_2O$ (mainly produced by the weathering of potash feldspar) is easily leached from primary minerals and is then absorbed by secondary clay minerals with ongoing weathering (Yang et al., 2006; Liang et al., 2013). In the arid and semi-arid regions of Asia, $K_2O$ is enriched in palaeosols compared to loess horizons (Yang et al., 2006). Thus, high $K_2O/Na_2O$ ratios are indicative of intense chemical weathering.

In the red clay-loess sequence of the CLP, magnetic parameters and the clay content are well correlated and thus are regarded as proxies of EASM strength (Liu et al., 2004). Aeolian particles usually have two distinct magnetic components, consisting of detrital and pedogenic material, respectively (Liu et al., 2004). $\chi_{lf}$ can reflect the combined susceptibility of both components, but changes in $\chi_{lf}$ are mainly affected by changes in the concentration of pedogenic magnetic grains (Liu et al., 2004). The grain-size distribution of pedogenic particles within the superparamagnetic (SP) to single-domain (SD) size range has been shown to be constant (Liu et al., 2004, 2005). Thus, $\chi_{fd}$ can be used detect SP minerals produced by pedogenesis and therefore the correlation coefficient between $\chi_{lf}$ and $\chi_{fd}$ is a measure of the contribution of such grains (<0.03 μm for magnetite) to the bulk susceptibility (Liu et al., 2004; Xia et al., 2014). As shown in Figure 4a, $\chi_{lf}$ is positively correlated with $\chi_{fd}$, which means that the magnetic susceptibility of the XSZ red clay mainly reflects pedogenic enhancement of the primary aeolian ferromagnetic content via the in-situ formation of fine-grained ferrimagnetic material. Thus, the magnetic susceptibility primarily reflects pedogenic intensity. Both the original and pedogenic magnetic signals can be separated using a simple linear regression method (Liu et al., 2004; Xia et al., 2014), which we use to extract the

307 lithogenic ($\chi_0$) and pedogenic magnetite/maghemite ($\chi_{pedo}$) components. We found that
308 pedogenic magnetite/maghemite accounts for 11% of the susceptibility ($\chi_{pedo} = \chi_{fd} / 0.11$).
309 Pedogenesis results in enhanced secondary clay formation (Sun and Huang, 2006b);
310 however, not all of the clay particles are derived from in situ pedogenesis, but rather are
311 inherited from aeolian transport and deposition. Clay particles can adhere to coarser silt and
312 sand particles (Sun and Huang, 2006b). In the western CLP, the coarse silt (>40 μm) content
313 is regarded as a rough proxy of winter monsoon strength (Wang et al., 2002). Therefore, to
314 eliminate this signal from the primary clay particles, the <2 μm/>40 μm ratio is proposed to
315 evaluate pedogenic intensity. Furthermore, the similarity of the variations of <2 μm/>40 μm
316 ratio and $\chi_{pedo}$ confirms that in this case <2 μm/>40 μm ratio has the potential to evaluate the
317 pedogenic intensity (Fig. 6).

318 **5.2 Time- and frequency- domain analysis of carbonate content and $\chi_{pedo}$**

319 The power spectral analyses of carbonate content and $\chi_{pedo}$ show different dominant
320 cycles (Fig. 5 a-b). In detail, $\chi_{pedo}$ is concentrated in the eccentricity (100 kyr), obliquity (41
321 kyr) and precession (21 kyr) bands and other periodicities (71 kyr and 27 kyr) are also
322 evident. By contrast, the carbonate signal is concentrated in the precession (21 kyr) and
323 obliquity (41 kyr) bands, but it also exhibits even more prominent periodicities of 56 kyr and
324 30 kyr. Furthermore, the fluctuations in $CaCO_3$, weathering and pedogenesis indices agree
325 well with orbital eccentricity variations during 4.7-3.9 Ma (Fig. 5 d). Three orbital
326 periodicities were also detected at other sites in CLP, in the interval from the late Miocene to
327 the early Pliocene, confirming that changes in orbital parameters had a substantial impact of
328 the climate of the CLP (Han et al., 2011).

King (1996) proposed that non-orbital cycles may originate from harmonic effects or interactions of the orbital cycles, while Lu (2004) ascribed them to unstable dust depositional processes followed by varying degrees of pedogenesis in palaeosol units. In the XSZ section, the deposition rate is low and uneven, which potentially resulted in the incomplete preservation of the paleoclimatic signal, especially for the relatively short precession cycles. In addition, pedogenesis and post-depositional compaction would also weaken the orbital signals and produce spurious cycles. Moreover, the carbonate content at various depths is affected by leaching which means that the record integrates soil polygenetic processes, thus obscuring orbital forcing trends related to precipitation amount. Therefore, we speculate that uneven and low deposition rate, combined with compaction and leaching processes, may have weakened the orbital signals and may be responsible for the presence of non-orbital cycles in the XSZ section.

To investigate the post-6.7 Ma frequency domain evolution of the climate signals in the XSZ section, we filtered the carbonate content and $\chi_{pedo}$ time series at the periods of 100, 41, and 21 kyr, using Gaussian band filters centered at frequencies of 0.01, 0.02439, and 0.04762, respectively. We then compared the results with the equivalent filtered components of the stacked deep-sea benthic oxygen isotope record. The results show that the fluctuations of the three filtered components (especially the 41-kyr component) of both proxies change from a low amplitude during 6.7-4.7 Ma to a relatively high amplitude during 4.7-3.9 Ma (Fig. 5 c). The enhanced orbital-scale variability of the two proxies from 4.7-3.9 Ma implies increased seasonality and wet-dry contrasts. This shift is not observed in the Earth orbital parameters but is observed in the filtered 41-kyr component of the stacked deep-sea benthic oxygen

isotope record ($\delta^{18}O$). This may mean that the enhancement of wet-dry contrasts at the XSZ site was not driven directly by changes in solar radiation intensity but rather was linked with changes in ice volume or global temperature.

### 5.3 Late Miocene-Pliocene climate history revealed by the Xiaoshuizi red clay

#### 5.3.1 Multi-proxy evidence for a dry climate during the late Miocene

We used the proxies of pedogenesis and chemical weathering to reconstruct the late Miocene and early Pliocene climatic history of the Xiaoshuizi planation surface. During the late Miocene, the relatively high carbonate values with minor fluctuations indicate that the climate was dry, and low Rb/Sr and $K_2O/Na_2O$ ratios also support the occurrence of weak chemical weathering. Notably, both the Rb/Sr and $K_2O/Na_2O$ ratios show opposite trends to that of carbonate content, meaning that low effective precipitation resulted in weak chemical weathering. Furthermore, the pedogenic proxies ($\chi_{pedo}$ and $\chi_{lf}$), characterised by low values with minor fluctuations, generally support the occurrence of weak pedogenesis under an arid climate. Thus, the climate at the XSZ site was relatively arid during this interval, resulting in weak chemical weathering and pedogenic intensity. However, there are several subtle differences between the carbonate and pedogenic indexes. It is evident that the carbonate content decreases with an increased amplitude of variation after 5.5 Ma, which is consistent with the cycles of carbonate nodules within paleososol horizons observed in the field (Li et al., 2017). It is possible that increased precipitation since 5.5 Ma induced eluviation and the redeposition of carbonate. However, the pedogenic indexes indicate that the generally arid climate was interrupted by two episodes of enhanced pedogenesis, at 5.85-5.7 Ma and 5.5-5.35 Ma. The subtle differences may result from differences in the sensitivity of magnetic

susceptibility and carbonate content to precipitation variability when precipitation is low (Sun et al., 2010). In addition, a coeval mollusk record from the western Liupanshan showed that cold-aridiphilous species dominated, which also indicates that cold and dry climatic conditions occurred in the western CLP during the late Miocene (Fig. 7 g).

Coeval pollen, mollusk and magnetic records from the central and eastern CLP also indicate generally dry and cold climatic conditions (Wang et al., 2006; Wu et al., 2006; Nie et al., 2014). However, the principal difference is that at the XSZ site, the arid climate was relatively stable, while the climate of the central and eastern CLP was interrupted by several humid stages. For example, two humid stages (6.2-5.8 Ma and 5.4-4.9 Ma) are recorded by the magnetic susceptibility of the red clay in the central and eastern CLP but are absent in the magnetic susceptibility record at the XSZ site (Fig. 7). Notably, the 41-kyr filtered component of thermo-humidiphilous species from Dongwan was damped in the late Miocene (Li et al., 2008). Similarly, the amplitude of the orbital periodicities, filtered from the XSZ carbonate content and $\chi_{pedo}$ records, was obviously damped during 6.7-4.7 Ma. However, the three periodicities in the Summer Monsoon index from the central CLP show no obvious difference between the late Miocene and Pliocene, but only a slight reduction in variability after 4.2 Ma (Sun et al., 2010). Therefore, we agree that a dry climate prevailed on the CLP during the late Miocene; however, the difference was that the climate in the central and eastern CLP fluctuated more substantially than was the case in the vicinity of the XSZ red clay section.

The especially damped response of the wet-dry climatic oscillations in the western CLP to obliquity forcing may indicate that the influence of the palaeo-EASM in the western CLP

was negligible. It is widely known that the summer monsoon intensity decreases from southeast to northwest across the CLP. A regional climate model experiment demonstrated that the modern East Asian Summer Monsoon was not fully established in the late Miocene and had only a small impact on northern China (Tang et al., 2011). A weak palaeo-EASM intensity from 7.0-4.8 Ma was revealed by hematite/goethite and smectite/kaolinite ratios at ODP Site 1148 in the South China Sea (SCS) (Fig. 7 i and j). Therefore, we infer that the palaeo-EASM was weak and had only a minor impact on the climate in the study region. In addition, previous studies indicated that the red clay may have been transported by both low-level northerly winds and the upper-level westerlies (Sun et al., 2004; Vandenberghe et al., 2004) and thus the impact of the westerly circulation on the study region cannot be ignored. Notably, the variation of the pedogenic proxies roughly parallels that of the stacked deep-sea benthic foraminiferal oxygen isotope curve (Fig. 6), and that $\chi_{pedo}$ has a positive relationship with $\delta^{18}O$ (Fig. 4 e). This indicates that when the global temperature was low, pedogenic intensity in the study area increased. It is unreasonable to conclude that precipitation in the study area was dominated by the palaeo-EASM and thus we speculate that, during the late Miocene, precipitation transported by the palaeo-EASM was limited and that the westerly circulation probably dominated the regional climate.

The simultaneous reduction in amplitude of the 41-kyr filtered components from the western CLP and the deep sea $\delta^{18}O$ record during the late Miocene likely indicates that the dry climate was related to changes in global temperature and ice volume. A sustained cooling occurred in both hemispheres during the late Miocene which culminated between 7 and 5.4 Ma (Herbert et al., 2016). $\delta^{18}O$ records from DSDP and ODP sites show an increase of ~1.0‰

during the late Miocene which resulted from the increased ice volume and the associated decrease in global temperature (Zachos et al., 2001). In the Northern Hemisphere, transient glaciations occurred when the cooling culminated (Herbert et al., 2016). Records from high-latitude regions of the Northern Hemisphere indicate continuously decreasing temperatures and increasing ice volume during the late Miocene (Jansen and Sjøholm, 1991; Mudie and Helgason, 1983; Haug et al., 2005). During the Quaternary, a dry climate prevailed during glacial periods when the global average temperature (especially in summer) was low. Cool summers could result in a small land-sea thermal contrast which in turn weakened the palaeo-EASM. Furthermore, the increased ice volume in the Northern Hemisphere resulted in an increased meridional temperature gradient (Herbert et al., 2016), thus strengthening the westerlies and driving them southwards. This would have prevented the northwestward penetration of the Asian Summer Monsoon, which is also proposed as the driving mechanism for a weak EASM in northern China during glacial periods (Sun et al., 2015). Thus, the southward shift of the westerlies had a significant impact on the XSZ region. However, moisture sources for the westerly air flow are distant from the CLP (Nie et al., 2014), and only a relatively small amount of moisture was carried to the CLP, resulting in a dry and stable climate in the XSZ region. In conclusion, global cooling and increasing ice volume in the Northern Hemisphere contributed to the dry climatic conditions in the study region.

**5.3.2 Intermittently humid climate during the early Pliocene**

During the early Pliocene, the proxy evidence indicates that the previously arid climate of the XSZ area became humid from ~4.7 Ma. The carbonate content was low on average but with large fluctuations, indicating that the climate was generally humid with increased dry-

wet oscillations, especially during 4.7-3.9 Ma. Several eluvial-illuvial cycles are evident during 4.7-3.9 Ma; the carbonate content in the eluvial horizons was less than 8%, whereas in illuvial horizons it was >21% (Fig. 6). Research on the migration process of carbonate indicate that a seasonally wet/dry climate is a key factor in driving carbonate dissolution and reprecipitation, and strong seasonally-biased precipitation enhances the leaching process and produces thick leached horizons (Rossinsky and Swart, 1993; Zhao, 1995, 1998). The occurrence of high-frequency cycles of carbonate eluviation-redeposition indicates that seasonal precipitation increased during this interval. Furthermore, the variations of Rb/Sr and $K_2O/Na_2O$ ratios are very similar to those of carbonate content, which suggests that weathering intensity was related to precipitation amount. Generally, high values of the <2 μm />40 μm ratio, $\chi_{pedo}$ and $\chi_{lf}$ correspond to large contrasts in carbonate content between eluvial and illuvial horizons; thus, increased precipitation had a significant influence on pedogenic intensity. Seasonal precipitation was intermittently enhanced from 4.7-3.9 Ma, and so was weathering and pedogenic intensity. Pedogenesis and weathering intensity reached a maximum during 4.60-4.25 Ma, as did precipitation intensity, manifested by the enhanced eluviation and carbonate accumulation. Notably, during this interval of peak precipitation (4.6-4.25 Ma), the enhancement of the <2 μm />40 μm ratio is not as strong as that of $\chi_{pedo}$, which may indicate that the former is of limited value when pedogenic intensity is strong. During 3.9-3.6 Ma, precipitation decreased, and weathering and pedogenic intensity also weakened. Consistent with the records of the XSZ section, mollusk records from Dongwan also indicate the occurrence of warm and humid conditions in the western CLP during the early Pliocene (Fig. 7 h).

Palynological and terrestrial mollusk records from the central CLP also indicate relatively humid conditions during the early Pliocene (Wang et al., 2006; Wu et al., 2006). Magnetic susceptibility records from the central and eastern CLP are similar to that from the XSZ section in that both the magnitude and the variability are high during the early Pliocene. From 4.1-3.9 Ma, the increased magnetic susceptibility indicates that humid climatic conditions prevailed across the entire CLP (Fig. 7). Evidently, when precipitation amount peaked in the vicinity of the XSZ section during 4.60-4.25 Ma, the magnetic susceptibility values at Xifeng, Lingtai and Chaona were low. However, a record of $Fe_2O_3$ ratio from Lingtai reveals extremely high values, corresponding to the presence of abundant clay coatings, during 4.8-4.1 Ma and this interval was interpreted as experiencing the strongest EASM intensity in the CLP since 7.0 Ma (Ding et al., 2001). In addition, the relative intensity of pedogenic alteration of the grain-size distribution was the strongest during the interval from 4.8-4.2 Ma in the Lingtai section (Sun et al., 2006c). Pollen assemblages at Chaona indicate a substantially warmer and more humid climate from 4.61-4.07 Ma (Ma et al., 2005). These various lines of evidence indicate that during 4.60-4.25 Ma the climate was warm and humid in the central CLP. Gleying has been implicated in reducing the value of magnetic susceptibility as a record of precipitation during this period (Ding et al., 2001). When soil moisture regularly exceeds the critical value, dissolution of ferrimagnetic minerals occurs and the susceptibility signal is negatively correlated with pedogenesis (Liu et al., 2003). This alone indicates that precipitation was likely to have been very high during this interval.

In summary, a wet climate prevailed across the CLP in the early Pliocene. At the same time, the hematite/goethite ratio in the sediments of the South China Sea also indicates

enhanced precipitation amount and the smectite/kaolinite ratio indicates increased seasonality at ~4.7 Ma (Fig. 7 i and j) and thus the enhancement of the palaeo-EASM (Clift et al., 2006, 2014). Therefore, we regard the climatic change evident in XSZ section to reflect the expansion of the palaeo-EASM.

Ding (2001) proposed that the uplift of the TP to a critical elevation resulted in an enhanced summer monsoon system during 4.8-4.1 Ma. TP uplift was shown to have had profound effects on the EASM in terms of its initiation and strength, as well as in changing the distribution of the band of high precipitation in East Asia (Li et al., 1991, 2014; An et al., 2001). A detailed modeling study demonstrated that the uplift of the northern TP mainly resulted in an intensified summer monsoon and increased precipitation in northeast Asia (Zhang et al., 2012). From 8.26-4.96 Ma, massive deltaic conglomerates were widely deposited and the sediment deposition rate increased, indicating the uplift of the Qilian Mountains (Song et al., 2001). At the same time, the Laji Mountains underwent pronounced uplift by thrusting at ~8 Ma, which resulted in the current basin-range pattern (Li et al., 1991; Fang et al., 2005a; Zheng et al., 2000). However, geological and palaeontological records indicate that the uplift of the eastern and northern margins of the TP was very minor from the late Miocene to the middle Pliocene (Li et al., 1991, 2015; Zheng et al., 2000; Fang et al., 2005a, 2005b). Therefore, we speculate that uplift of the TP was not the major cause of the expansion of the palaeo-EASM at ~4.7 Ma.

The occurrence of a humid climate across the CLP was synchronous with the gradual closure of the Panama Seaway (Keigwin, 1978; O'Dea et al., 2016). Nie (2014) proposed that the freshening of Eastern Equatorial and North Pacific surface water, resulting from the

505 closure of the Panama Seaway since 4.8 Ma (Haug et al., 2001), led to sea ice formation in
506 the North Pacific Ocean, which enhanced the high-pressure cell over the Pacific and
507 increased the strength of southerly and southeasterly winds. However, there was a warming
508 trend in the Northern Hemisphere from 4.6 Ma (Haug et al., 2005; Lawrence et al., 2006).
509 The gradual closure of the Panama Seaway resulted in the reorganization of surface currents
510 in the Atlantic Ocean. Notably, the Gulf Stream was enhanced and began to transport warm
511 surface waters to high northern latitudes, thus strengthening the Atlantic meridional
512 overturning circulation and warming the Arctic (Haug and Tiedemann, 1998; Haug et al.,
513 2005). Three independent proxies from an early Pliocene peat deposit in the Canadian High
514 Arctic indicate that Arctic temperatures were 19 ℃ warmer during the early Pliocene than
515 today (Ballantyne et al., 2010). This warmth is also confirmed by other records from high
516 northern latitude regions: diatom abundances and assemblages, pollen data, magnetic
517 susceptibility and sedimentological evidence from Siberia all indicate that the climate was
518 warm and wet in the early Pliocene (Baikal Drilling Project Memb, 1997, 1999). Furthermore,
519 a decrease in the input of ice-rafted debris to the sediments of the subarctic northwest Pacific
520 was synchronous with the expansion of the palaeo-EASM during the early Pliocene (Fig. 6).
521 The warming of the Northern Hemisphere and external heating derived from a reduced ice
522 albedo at high northern latitudes enhanced the thermal contrast between the Pacific and
523 Eurasian regions (Dowsett et al., 2010). This large land-ocean thermal contrast was essential
524 for enhancing the palaeo-EASM. On the other hand, the unusually warm high northern
525 latitudes and the West Antarctic ice-sheet expansion by 6–5 Ma (Zachos et al., 2001, 2008)
526 steepened interhemispheric thermal gradient and further caused the thermal equator to move

northward (Chiang and Friedman, 2012; Broecker and Putnam, 2013). This facilitated the northwestward expansion of the palaeo-EASM, which is also proposed as the driving mechanism for northwestward migration of the monsoon rain belt for the warm Holocene (Yang et al., 2015). Therefore, we infer that the warming of high northern latitudes in response to the closure of the Panamanian Seaway may have facilitated the expansion of the palaeo-EASM during the early Pliocene. However, there are several uncertainties associated with such an explanation. For example, the timing of the closure of the Panama Seaway is still debated (Bacon et al., 2015; O'Dea et al., 2016), and it is unclear how strongly these changes influenced the palaeo-EASM. Addressing these questions requires more geological evidence and precise model simulations of the early Pliocene climate. The value of our study lies in proposing the potential linkage of the evolution of palaeo-EASM and changes in temperatures of high northern latitudes during the early Pliocene.

## 6. Conclusions

The continuous late Miocene-Pliocene red clay sequence preserved on the planation surface in the NE Tibetan Plateau provides the opportunity to elucidate the history of the Asian monsoon in the western CLP. Multi-proxy records from the XSZ section, together with other paleoclimatic records from the CLP, reveal the major patterns of climatic change from 6.7-3.6 Ma. During the late Miocene, both the amount and variability of precipitation over the XSZ section were small; however, they were much greater in the central and eastern CLP; thus, the palaeo-EASM had little influence on the climate of the western CLP at this time. During the early Pliocene, the records from the XSZ section indicate that both the amount and variability of precipitation increased from 4.7-3.9 Ma. The climate was characterized by

abrupt increases in the seasonality of precipitation, which attests to a major northwestward extension and enhancement of the summer monsoon. Multiple paleoclimatic proxies clearly show that the strongest summer monsoon occurred during 4.60-4.25 Ma. The expansion of the palaeo-EASM may have been caused by warming of the high northern latitudes in response to the closure of the Panamanian Seaway during the early Pliocene.


## Acknowledgements

We thank Ai Song, Jia Liu, Shanpin Liu and Jun Zhang for the drilling operation and Fengxia Yu for her early experimental work. We thank Jan Bloemendal for modifying and polishing the language. We specially thank Ran Feng and four anonymous reviewers for their suggestions and comments that have helped improve the paper. This work was supported by the National Natural Science Foundation of China (grants 41330745 and 41401214) and the Key Laboratory of Continental Collision and Plateau Uplift, Institute of Tibetan Plateau Research (LCP201602).


## References


An, Z. S., Kutzbach, J. E., Prell, W. L., Porter, S. C.: Evolution of Asian monsoons and phased uplift of the Himalayan Tibetan plateau since late Miocene times. Nature, 411, 62–66, 2001.

An, Z. S.: Late Cenozoic climate change in Asia. Springer Netherlands, 2014.

Ao, H., Roberts, A. P., Dekkers, M. J., Liu, X., Rohling, E. J., Shi, Z., An, Z. S., and Zhao, X.: Late Miocene–Pliocene Asian monsoon intensification linked to Antarctic ice-sheet growth. Earth & Planetary Science Letters,444, 75-87, 2016.

571 Avery, B. W., and Bascomb, C. L.: Soil survey laboratory methods, 1974.

572 Bacon, C. D., Silvestro, D., Jaramillo, C., Smith, B. T., Chakrabarty, P., and Antonelli, A.: Biological
573 evidence supports an early and complex emergence of the Isthmus of Panama. Proceedings of the
574 National Academy of Sciences,112(19), 6110-6115, 2015.

575 Baikal Drilling Project Memb.: Preliminary results of the first scientific drilling on lake Baikal,
576 Buguldeika site, southeastern Siberia. Quaternary International, 37(2), 3-17, 1997.

577 Baikal Drilling Project Memb.: Continuous paleoclimate record recovered for last 5 million years. Eos
578 Transactions American Geophysical Union, 78(51), 597-601, 1999.

579 Ballantyne, A. P., Greenwood, D. R., SinninghеDamste, J. S., Csank, A. Z., Eberle, J. J., and Rybczynski,
580 N.: Significantly warmer Arctic surface temperatures during the Pliocene indicated by multiple
581 independent proxies. Geology, 38(7), 603-606, 2010.

582 Brierley, C. M., Fedorov, A. V., Liu, Z., Herbert, T. D., Lawrence, K. T., and Lariviere, J. P.: Greatly
583 expanded tropical warm pool and weakened Hadley circulation in the early Pliocene. Science,
584 323(5922), 1714-8, 2009.

585 Brierley, C. M., and Fedorov, A. V.: Relative importance of meridional and zonal sea surface temperature
586 gradients for the onset of the ice ages and Pliocene-Pleistocene climate evolution. Paleoceanography,
587 25(4), 2010.

588 Broecker, W.S., Putnam A.E.: Hydrologic impacts of past shifts of Earth's thermal equator offer insight
589 into those to be produced by fossil fuel $CO_2$. Proc Natl Acad Sci USA 110(42):16710–16715, 2013.

590 Buggle, B., Glaser, B., Hambach, U., Gerasimenko, N., and Markovi, S.: An evaluation of geochemical
591 weathering indices in loess–paleosol studies. Quaternary International, 240(1–2):12-21, 2011.

592 Chiang J. C. H., Friedman A. R.: Tropical cooling, interhemispheric thermal gradients, and tropical climate

593 change. Annu Rev Earth Planet Sci 40(1):383–412, 2012.
594 Chang, H., An, Z. S., Wu, F. L., Jin, Z., Liu, W. G., and Song, Y. G.: A Rb/Sr record of the weathering
595 response to environmental changes in westerly winds across the Tarim basin in the late Miocene to
596 the early Pleistocene. Palaeogeography Palaeoclimatology Palaeoecology, 386(6), 364-373, 2013.
597 Clift, P. D.: Controls on the erosion of Cenozoic Asia and the flux of clastic sediment to the ocean. Earth
598 & Planetary Science Letters, 241(3–4), 571-580, 2006.
599 Clift, P. D., Hodges, K. V., Heslop, D., Hannigan, R., Long, H. V., and Calves, G.: Correlation of
600 Himalayan exhumation rates and Asian monsoon intensity. Nature Geoscience, 1(12),
601 doi:10.1038/ngeo351, 2008.
602 Clift, P. D., Wan, S. M., and Blusztajn, J.: Reconstructing chemical weathering, physical erosion and
603 monsoon intensity since 25 Ma in the northern South China Sea: a review of competing
604 proxies. Earth-Science Reviews, 130 (3), 86-102, 2014.
605 Compo, G., Whitaker, J., Sardeshmukh, P., and Mccoll, C.: The quality control system of the 20th century
606 reanalysis dataset. Egu General Assembly, 15, 2013.
607 Ding, Z. L., Yang, S. L., Sun, J. M., and Liu, T. S.: Iron geochemistry of loess and red clay deposits in the
608 Chinese Loess plateau and implications for long-term Asian monsoon evolution in the last 7.0
609 Ma. Earth & Planetary Science Letters, 185(1), 99-109, 2001.
610 Dowsett, H. J., Robinson, M., Haywood, A., Salzmann, U., Hill, D., Sohl, L. E., Chandler, M., Williams,
611 M., Foley, K., and Stoll, D. K.: The PRISM3D paleoenvironmental reconstruction. Stratigraphy, 7,
612 123-139, 2010.
613 Fedorov, A. V., Brierley, C. M., Lawrence, K. T., Liu, Z., Dekens, P. S., and Ravelo, A. C.: Patterns and
614 mechanisms of early Pliocene warmth. Nature, 496 (7443), 43, 2013.

615 Fang, X. M, Li, J. J, Derbyshire, E., Fitzpatrick, E. A., and Kemp, R. A.: Micromorphology of the Beiyuan
616 loess-paleosol sequence in Gansu province, China: geomorphological and paleoenvironmental
617 significance. Palaeogeography Palaeoclimatology Palaeoecology, 111(3–4), 289-303, 1994.
618 Fang, X. M., Ono, Y., Fukusawa, H., Pan, B. T., Li, J. J., Guan, D. H., Oi. K., Tsukamotoc, S., Torii, M.,
619 and Mishima, T.: Asian summer monsoon instability during the past 60,000 years: magnetic
620 susceptibility and pedogenic evidence from the western Chinese Loess plateau. Earth & Planetary
621 Science Letters, 168(3–4), 219-232, 1999.
622 Fang, X. M., Yan, M. D., Voo, R. V. D., Rea, D. K., Song, C. H., Parés, J. M., Gao J. P., Nie J. S., and Dai
623 S: Late Cenozoic deformation and uplift of the NE Tibetan plateau: evidence from high-resolution
624 magnetostratigraphy of the Guide basin, Qinghai province, China. Geological Society of America
625 Bulletin, 117(9), 1208-1225, 2005a.
626 Fang, X., Zhao, Z. J., Li J. J., Yan, M. D, Pan, B. T., Song, C. H., and Dai, S.: Magnetostratigraphy of the
627 late Cenozoic Laojunmiao anticline in the northern Qilian mountains and its implications for the
628 Northern Tibetan plateau uplift. Science in China, 48(7), 1040-1051, 2005b.
629 Fang, X. M, Wu, F. L., Hai, W. X., Wang, Y. D., Zhang, X. Z., and Zhang, W. L.: Plio-Pleistocene drying
630 process of Asian inland-sporopollen and salinity records from Yahu section in the central Qaidam
631 basin (in Chinese). Quaternary Sciences 28(5): 874-882, 2008.
632 Fedo, C. M., Nesbitt, H. W., and Young, G. M.: Unraveling the effects of potassium metasomatism in
633 sedimentary rocks and paleosols, with implications for paleoweathering conditions and
634 provenance. Geology, 23(10), 921-924, 1995.
635 Guo, Z. T., Peng, S. Z., Hao, Q. Z., Biscaye, P. E., and Liu, T. S.: Origin of the Miocene–Pliocene red-
636 earth formation at Xifeng in northern China and implications for paleoenvironments.

637 Palaeogeography Palaeoclimatiology Palaeoecology, 170(1-2), 11-26, 2001.
638 Han, W., Fang, X., Berger, A., and Yin, Q.: An astronomically tuned 8.1 Ma eolian record from the
639 Chinese Loess plateau and its implication on the evolution of Asian monsoon. Journal of Geophysical
640 Research Atmospheres, 116 (D24114), 2011.
641 Haug, G. H., and Tiedemann, R.: Effect of the formation of the isthmus of Panama on Atlantic ocean
642 thermohaline circulation. Nature, 393 (3), 673-676, 1998.
643 Haug, G. H., Tiedemann, R., Zahn, R., and Ravelo, A. C.: Role of Panama uplift on oceanic freshwater
644 balance. Geology, 29(3), 207-210, 2001.
645 Haug, G. H., Ganopolski, A., Sigman, D. M., Rosell-Mele, A., Swann, G. E., Tiedemann, R., Jaccard, S. L.,
646 Bollmann, B. J., Maslin, M. A., Leng, M. J., and Eglinton, G.: North pacific seasonality and the
647 glaciation of north America 2.7 million years ago. Nature, 433(7028), 821-825, 2005.
648 He, T., Chen, Y., Balsam, W., Qiang. X.K., Liu, L.W., Chen, J., Li, F.J.: Carbonate leaching processes in
649 the Red Clay Formation, Chinese Loess plateau: Fingerprinting East Asian summer monsoon
650 variability during the late Miocene and Pliocene. Geophysical Research Letters, 40(1):194-198, 2013.
651 Herbert, T. D., Peterson, and Liu, Z.: Tropical ocean temperatures over the past 3.5 million
652 years. Science, 328(5985), 1530-4, 2010.
653 Herbert, T. D., Lawrence, K. T., Tzanova, A., Peterson, L. C., Caballerogill, R., and Kelly, C. S.: Late
654 Miocene global cooling and the rise of modern ecosystems. Nature Geoscience, 9(11), 2016.
655 Jansen, E., and Sjøholm, J.: Reconstruction of glaciation over the past 6 Myr from ice-borne deposits in the
656 Norwegian sea. Nature,349(6310), 600-603, 1991.
657 Keigwin, L. D.: Pliocene closing of the isthmus of Panama, based on biostratigraphic evidence from
658 nearby Pacific ocean and Caribbean sea cores. Geology, 6(10), 630, 1978.

King, T.: Quantifying non-linearity and geometry in time series of climate. Quaternary Science Reviews 15, 247-266, 1996.

Laskar, J.: Long-term solution for the insolation quantities of the earth. Proceedings of the International Astronomical Union, 2(14), 101-106, 2004.

Lawrence, K. T., Liu, Z., and Herbert, T. D.: Evolution of the eastern tropical pacific through Plio-Pleistocene glaciation. Science, 312(5770), 79-83, 2006.

Liang, L., Sun, Y., Beets, C. J., Prins, M. A., Wu, F., and Vandenberghe, J.: Impacts of grain size sorting and chemical weathering on the geochemistry of Jingyuan loess in the northwestern Chinese Loess plateau. Journal of Asian Earth Sciences, 69(12), 177-184, 2013.

Li, F. J., Rousseau, D. D., Wu, N., Hao, Q., and Pei, Y.: Late Neogene evolution of the East Asian monsoon revealed by terrestrial mollusk record in western Chinese Loess plateau: from winter to summer dominated sub-regime. Earth & Planetary Science Letters, 274(3–4), 439-447, 2008.

Li, J. J.: The environmental effects of the uplift of the Qinghai-Xizang plateau. Quaternary Science Reviews, 10(6), 479-483, 1991.

Li, J. J., Fang, X., Song, C., Pan, B., Ma, Y., and Yan, M., Late Miocene–quaternary rapid stepwise uplift of the NE Tibetan plateau and its effects on climatic and environmental changes. Quaternary Research, 81(3), 400-423, 2014.

Li, J. J., Zhou, S. Z., Zhao, Z. J., and Zhang, J.: The Qingzang movement: the major uplift of the Qinghai-Tibetan plateau. Science China Earth Sciences, 58(11), 2113-2122, 2015.

Li, J. J., Ma, Z. H., Li, X. M., Peng, T. J., Guo, B. H., Zhang, J., Song, C. H., Liu, J. Hui, Z. C., Yu, H., Ye, X. Y., Liu, S. P., Wang, X. X.: Late Miocene-Pliocene geomorphological evolution of the Xiaoshuizi peneplain in the Maxian Mountains and its tectonic significance for the northeastern

Tibetan plateau. Geomorphology. 295 393-405, 2017.

Liu, X. M., Rolph, T., An, Z., and Hesse, P.: Paleoclimatic significance of magnetic properties on the red clay underlying the loess and paleosols in China. Palaeogeography Palaeoclimatology Palaeoecology, 199(1), 153-166, 2003.

Liu, C. Q., Masuda, A., Okada, A., Yabuki, S., Zhang, J., and Fan, Z. L.: A geochemical study of loess and desert sand in northern China: implications for continental crust weathering and composition. Chemical Geology, 106 (3-4), 359-374, 1993.

Liu, Q., Jackson, M. J., Yu, Y., Chen, F., Deng, C., and Zhu, R.: Grain size distribution of pedogenic magnetic particles in Chinese loess/paleosols. Geophysical Research Letters, 312(22), 359-393, 2004.

Liu, Q., Torrent, J., Maher, B. A., Yu, Y., Deng, C. L., Zhu, R., and Zhao X. X.: Quantifying grain size distribution of pedogenic magnetic particles in Chinese loess and its significance for pedogenesis. Journal of Geophysical Research Atmosphere, 110(B11), 2005.

Liu, W., Liu, Z., An, Z. S., Sun, J., Chang, H., Wang, N., and Dong, J. B.: Late Miocene episodic lakes in the arid Tarim basin, western China. Proceedings of the National Academy of Sciences, 111(46), 16292-6, 2014.

Lu, H. Y., Zhang, F., Liu, X., and Duce, R. A: Periodicities of palaeoclimatic variations recorded by loess-paleosol sequences in China. Quaternary Science Reviews, 23(18–19), 1891–1900, 2004.

Ma, Y. Z., Wu, F. L., Fang, X. M., Li, J. J., An, Z. S., and Wei, W.: Pollen record from red clay sequence in the central Loess plateau between 8.10 and 2.60 Ma. Chinese Science Bulletin, 50(19), 2234-2243, 2005.

Mudie, P. J., and Helgason, J.: Palynological evidence for Miocene climatic cooling in eastern iceland about 9.8 myr ago. Nature, 303(5919), 689-692, 1983.

Nesbitt, H. W., Markovics, G., and Price, R. C.: Chemical processes affecting alkalis and alkaline earths during continental weathering. Geochimica Et Cosmochimica Acta, 44(11), 1659-1666, 1980.

Nie, J. S., Stevens, T., Song, Y., King, J. W., Zhang, R., Ji, S. C, Gong L. S., and Cares, D.: Pacific freshening drives Pliocene cooling and Asian monsoon intensification. Scientific Reports, 4, 5474, 2014.

O'Dea, A., Lessios H. A., Coates, A. G., Eytan, R. I., Restrepo-Moreno, S. A., Cione, A. L., Collins, L. S., Queiroz, A. D., Farris, D. W., Norris, R. D., Stallard, R. F., Woodburne, M. O., Aguilera, O., Aubry, M. P., Berggren, W. A., Budd, A. F., Cozzuol, M. A., Coppard, S. E., Duque-Caro, H., Finnegan, S., Gasparini, G. M., Grossman, E. L., Johnson, K. G., Keigwin, L. D., Knowlton, N., Leigh, E. G., Leonard-Pingel, J. S., Marko, P. B., Pyenson, N. D., Rachello-Dolmen, P. G., Soibelzon, E., Soibelzon, L., Todd, J. A., Vermeij, G. J., and Jackson, J. B. C.: Formation of the Isthmus of Panama. Science Advances, 2(8), 2016.

Pagani, M., Liu, Z., Lariviere, J., and Ravelo, A. C.: High earth-system climate sensitivity determined from Pliocene carbon dioxide concentrations. Nature Geoscience, 3(1), 27-30, 2010.

Rossinsky V. J., and Swart, P. K.,: Influence of climate on the formation and isotopic composition of calcretes. In: Swart, P.K., Lohmann, K.C., McKenzie, J., Savin, S. (Eds.), Climate Change in Continental Isotopic Records, American Geophysical Union: Geophysical Monography, 78, pp. 67-75, 1993.

Song, C. H., Fang, X. M., Li, J. J., Gao, J., Zhao, Z. J., and Fan, M. J.,: Tectonic uplift and sedimentary evolution of the Jiuxi basin in the northern margin of the Tibetan plateau since 13 Ma BP. Science China Earth Sciences,44(1), 192-202, 2001.

Song, Y. G., Fang, X. M., Torii, M., Ishikawa, N., Li, J. J., and An, Z. S.: Late Neogene rock magnetic record of climatic variation from Chinese eolian sediments related to uplift of the Tibetan

plateau. Journal of Asian Earth Sciences, 30(2), 324-332, 2007.

Sun, D. H., Bloemendal, J., Rea, D. K., An, Z. S., Vandenberghe, J.,and Lu, H., Su, R. X., and Liu, T.: . Bimodal grain-size distribution of Chinese loess, and its palaeoclimatic implications. Catena, 55(3), 325-340, 2004.

Sun, J. M., and Liu, T. S. : The age of the Taklimakan desert. Science, 312 (5780), 1612-1621, 2006a.

Sun, J. M., and Huang, X.: Half-precessional cycles recorded in Chinese loess: response to low-latitude insolation forcing during the last interglaciation. Quaternary Science Reviews, 25(9–10), 1065-1072, 2006b.

Sun, J. M., Liu, W. G., Liu, Z., Deng, T., Windley, B. F., and Fu, B.: Extreme aridification since the beginning of the Pliocene in the Tarim basin, western China. Palaeogeography Palaeoclimatology Palaeoecology, 2017.

Sun, Y. B., Lu, H. Y., and An, Z S.: Grain size of loess, palaeosol and red clay deposits on the Chinese Loess plateau: significance for understanding pedogenic alteration and palaeomonsoon evolution. Palaeogeography Palaeoclimatology Palaeoecology, 241(1), 129-138, 2006c.

Sun, Y. B., An, Z. S., Clemens, S. C., Bloemendal, J., and Vandenberghe, J.: Seven million years of wind and precipitation variability on the Chinese Loess plateau. Earth & Planetary Science Letters, 297(3–4), 525-535, 2010.

Sun, Y. B., Kutzbach, J., An, Z., Clemens, S., Liu, Z., Liu, W., Liu, X. D., Shi, Z. G., Zheng, W. P., Liang, L., Yan, Y., and Li, Y.: Astronomical and glacial forcing of East Asian summer monsoon variability. Quaternary Science Reviews, 115, 132-142, 2015.

Tripati, A. K., Roberts, C. D., and Eagle, R. A.: Coupling of $CO_2$ and ice sheet stability over major climate transitions of the last 20 million years. Science, 326(5958), 1394-1397, 2009.

748 Tang, H., Micheels, A., Eronen, J., and Fortelius, M.: Regional climate model experiments to investigate
749 the Asian monsoon in the late Miocene. Climate of the Past, 7(3), 847-868, 2011.
750 Vandenberghe, J., H. Lu, D. Sun, J. Huissteden, V., and Konert, M.: The late Miocene and Pliocene
751 climate in East Asia as recorded by grain size and magnetic susceptibility of the Red Clay deposits
752 (Chinese Loess Plateau), Palaeogeography Palaeoclimatology Palaeoecology, 204, 239–255,
753 doi:10.1016/S0031-0182(03)00729-6, 2004.
754 Wan, S. M., Tian, J., Steinke, S., Li, A., and Li, T.: Evolution and variability of the East Asian summer
755 monsoon during the Pliocene: evidence from clay mineral records of the South China
756 Sea. Palaeogeography Palaeoclimatology Palaeoecology, 293(1–2), 237-247, 2010.
757 Wang, H. B., Chen, F. H., and Zhang, J. W.: Environmental significance of grain size of loess-paleosol
758 sequence in western part of Chinese Loess plateau. Journal of Desert Research, 22(1), 21-26, 2002.
759 Wang, L., Lu, H. Y., Wu, N. Q., Li, J., Pei, Y. P., Tong, G. B., and Peng, S. Z.:. Palynological evidence for
760 Late Miocene-Pliocene vegetation evolution recorded in the red clay sequence of the central Chinese
761 Loess plateau and implication for palaeo-environmental change. Palaeogeography Palaeoclimatology
762 Palaeoecology. 241, 118–128, 2006.
763 Wara, M. W., Ravelo, A. C., and Delaney, M. L.: Permanent EI niño-like conditions during the Pliocene
764 warm period. Science, 309(5735), 758-61, 2005.
765 Watanabe, T., Suzuki, A., Minobe, S., Kawashima, T., Kameo, K., &Minoshima, K., Aguilar, Y. M., Wan,
766 R., Kawahata, H., Sowa, K., Nagai, T., and Kase, T.: Permanent EI niño during the Pliocene warm
767 period not supported by coral evidence. Nature, 471 (7337), 209-211, 2011.
768 Wu, N., Pei, Y., Lu, H., Guo, Z., Li, F., and Liu, T.: Marked ecological shifts during 6.2–2.4 Ma revealed
769 by a terrestrial molluscan record from the Chinese red clay formation and implication for

770 palaeoclimatic evolution. Palaeogeography Palaeoclimatology Palaeoecology, 233(3-4), 287-299,
771 2006.
772 Xia, D. S., Jia, J., Li, G., Zhao, S., Wei, H. T., and Chen, F. H.: Out-of-phase evolution between summer
773 and winter East Asian monsoons during the Holocene as recorded by Chinese loess deposits.
774 Quaternary Research, 81(3), 500-507, 2014.
775 Yang, S. L., Ding, F., and Ding, Z. L.: Pleistocene chemical weathering history of Asian arid and semi-arid
776 regions recorded in loess deposits of China and Tajikistan. Geochimica Et Cosmochimica Acta, 70(7),
777 1695-1709, 2006.
778 Yang, S. L., Ding, Z.L., Li, Y.Y., Wang, X., Jiang, W.Y., Huang, X.F.: Warming-induced northwestward
779 migration of the East Asian monsoon rain belt from the Last Glacial Maximum to the mid-Holocene.
780 Proc. Natl. Acad. Sci. USA 112, 13178–13183, 2015.
781 Zachos, J., Pagani, M., Sloan, L., Thomas, E., and Billups, K.: Trends, rhythms, and aberrations in global
782 climate 65 Ma to present. Science, 292(5517), 686-93, 2001.
783 Zachos, J.C., Dickens, G.R., Zeebe, R.E.: An early Cenozoic perspective on green-house warming and
784 carbon-cycle dynamics. Nature.451, 279–283, 2008.
785 Zhang, R., Jiang, D. B., Liu, X. D., and Tian, Z. P.: Modeling the climate effects of different subregional
786 uplifts within the Himalaya-Tibetan plateau on Asian summer monsoon evolution. Science
787 Bulletin, 57(35), 4617-4626, 2012.
788 Zhang, Y. G., Pagani, M., and Liu, Z.: A 12-million-year temperature history of the tropical Pacific
789 ocean. Science, 344(6179), 84, 2014.
790 Zhao, J. B.: A study of the $CaCO_3$ illuvial horizons of paleosols and permeated pattern far rain water (in
791 Chinese), J Geogr Sci, 15(4), 344-350, 1995.

792 Zhao, J. B.: Illuvial $CaCO_3$ layers of paleosol in loess and its environmental significance (in Chinese),
793 Journal of Xi'an Engineering University, 20(3), 46-49, 1998.
794 Zheng, H. B, Mcaulay Powell, C., An, Z. S., Zhou, J., and Dong, G. R.: Pliocene uplift of the northern
795 Tibetan plateau. Geology, 28(8), 715, 2000.
796

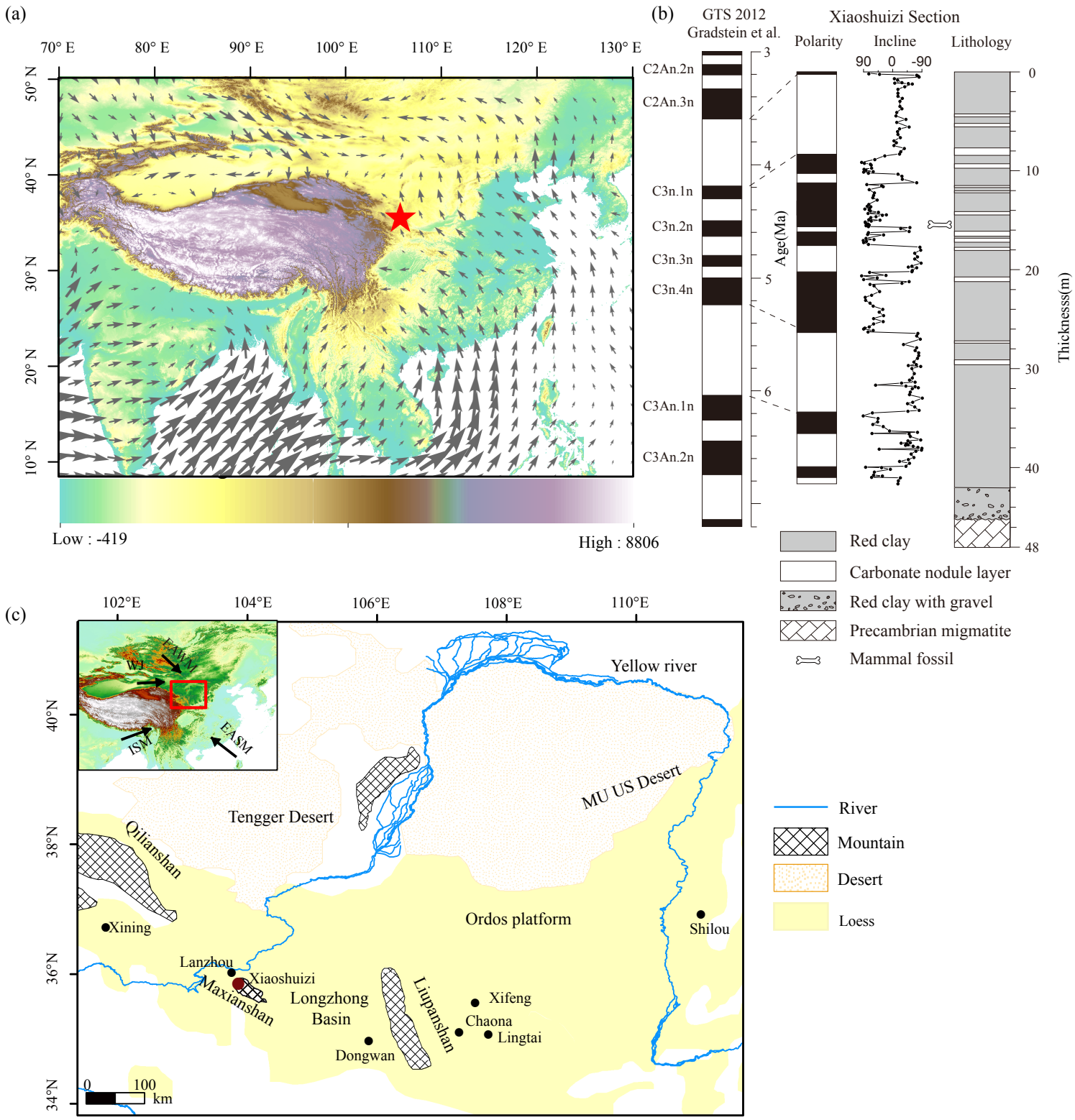


Fig. 1. Location of the study area and atmospheric circulation patterns. (a) 850 hPa vector wind averaged from June to August for 1982-2012 based on NOAA Earth System Research Laboratory reanalysis data (Compo et al., 2013). (b) Lithology and magnetostratigraphy of the XSZ drill core. (c) The Chinese Loess Plateau with locations of the studied Xiaoshuizi site and other sections mentioned in the text.

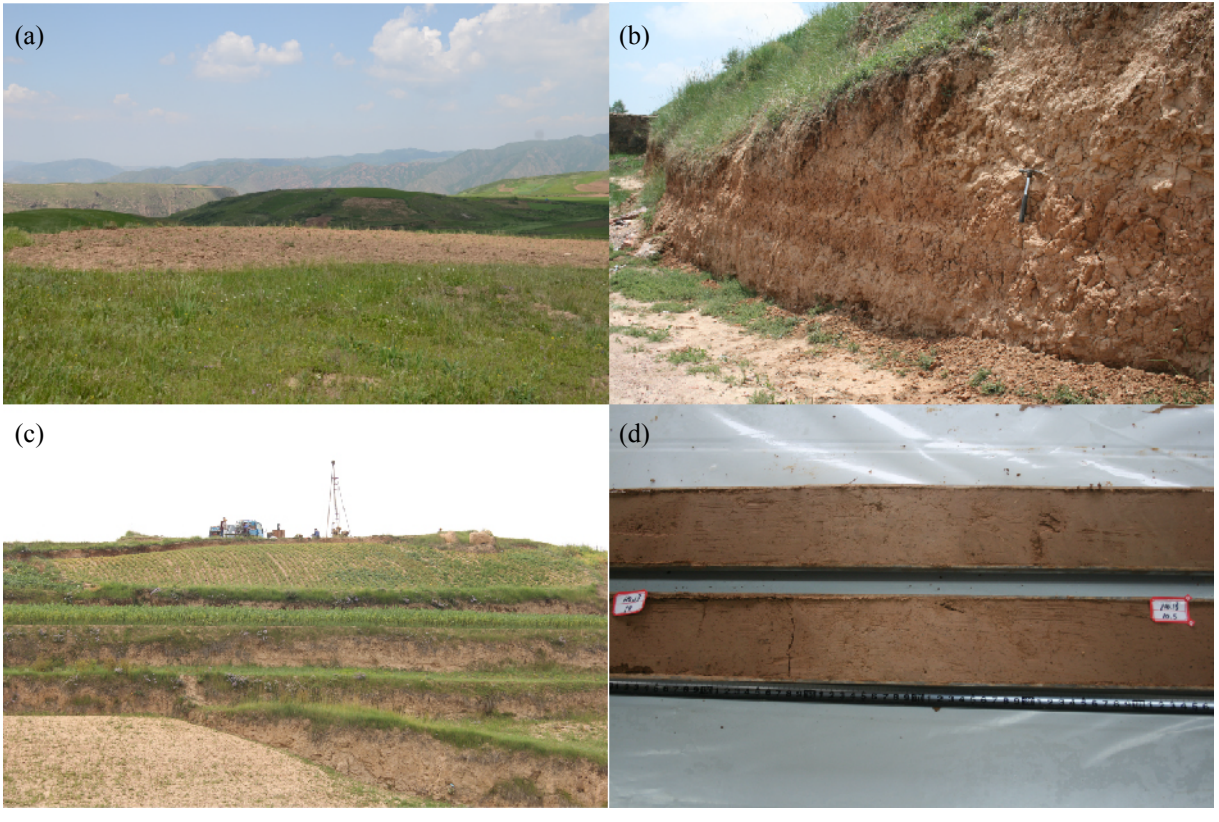
(a)
(b)
(c)
(d)

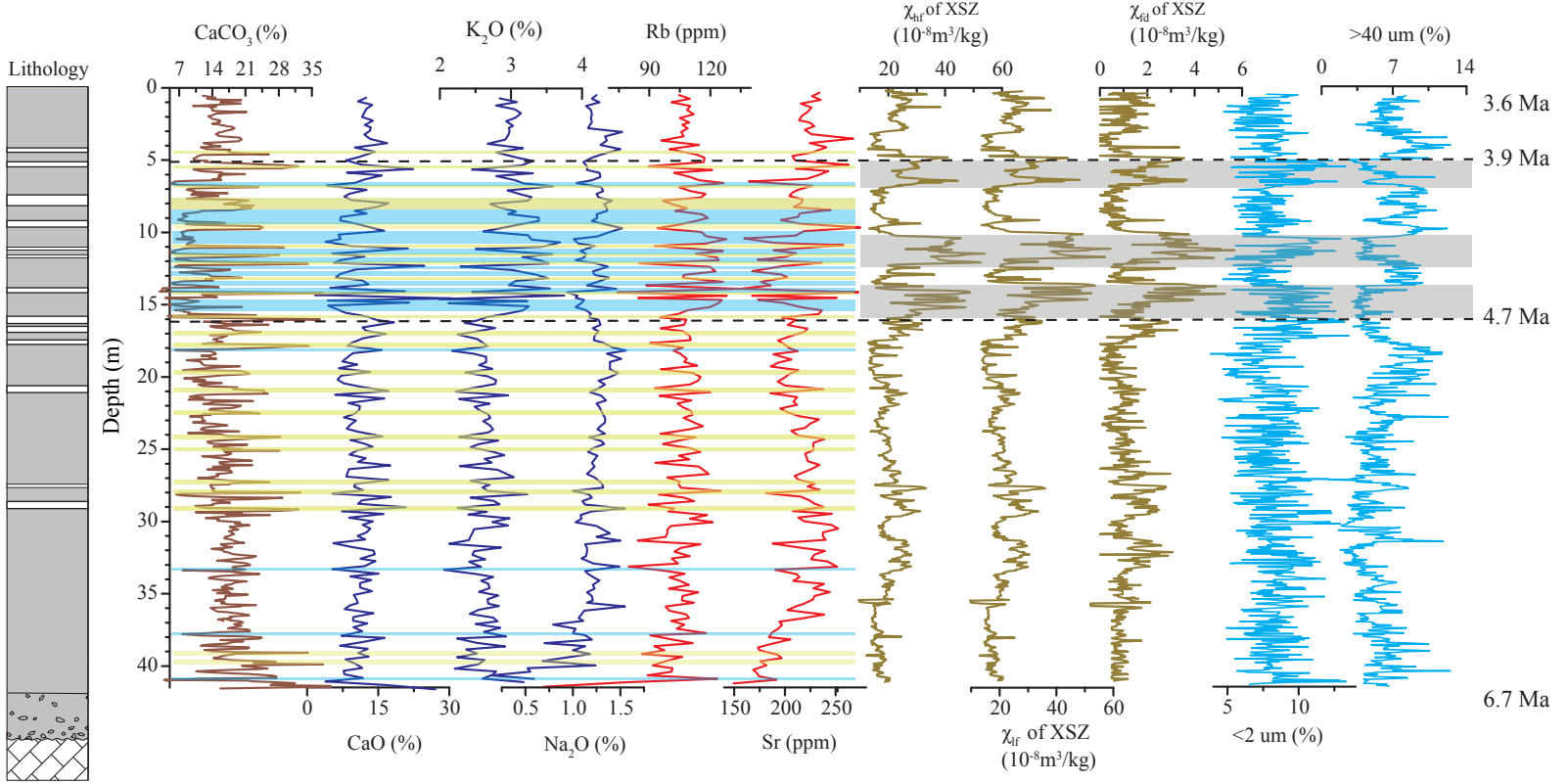
Lithology
Depth (m)
CaCO3 (%)
K2O (%)
Rb (ppm)
χhf of XSZ (10-8m3/kg)
χfd of XSZ (10-8m3/kg)
>40 um (%)
3.6 Ma
3.9 Ma
4.7 Ma
6.7 Ma
CaO (%)
Na2O (%)
Sr (ppm)
χlf of XSZ (10-8m3/kg)
<2 um (%)

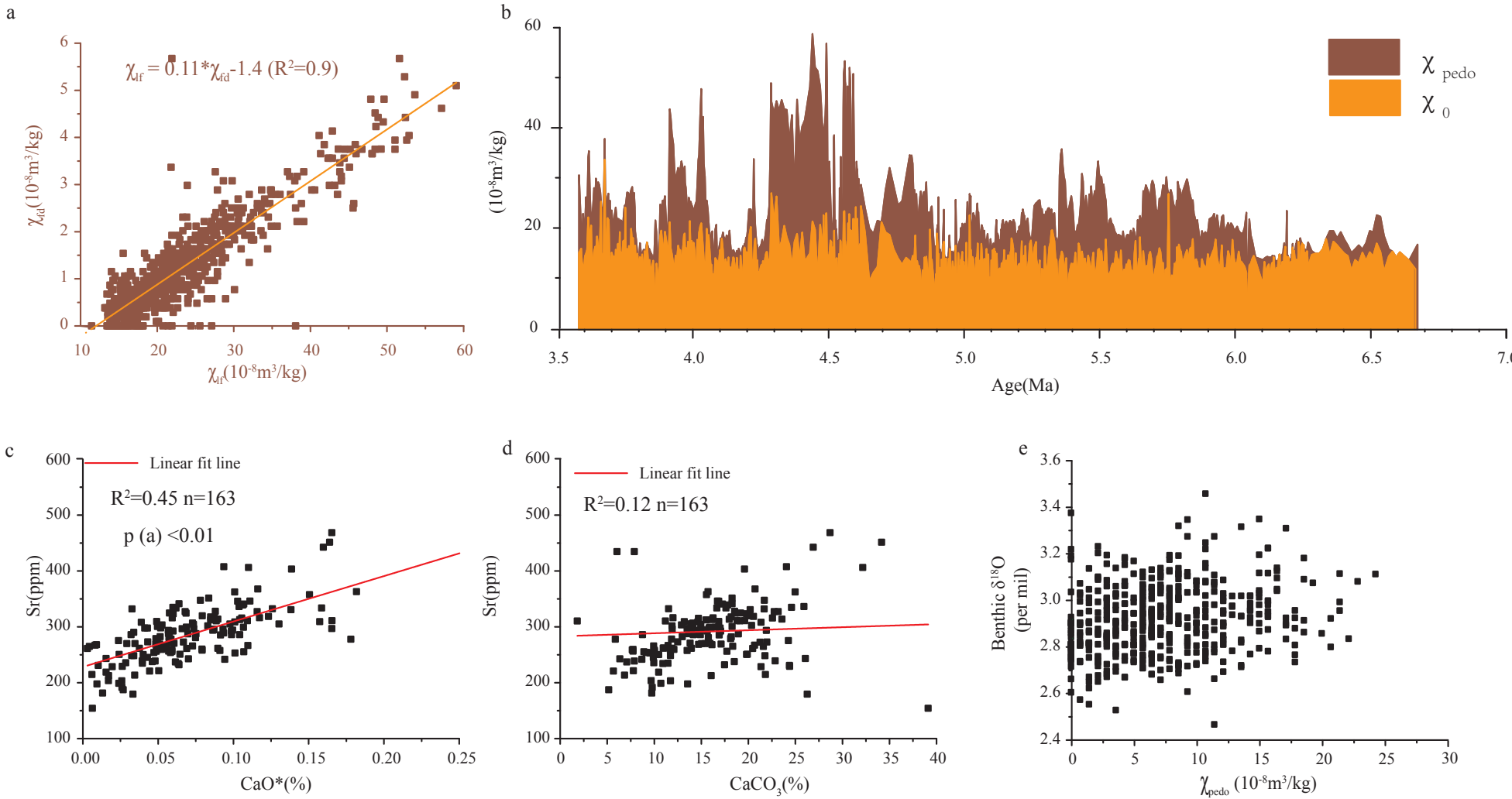
a
$\chi_{lf} = 0.11*\chi_{fd}-1.4$ ($R^2$=0.9)
$\chi_{fd}(10^{-8}m^3/kg)$
$\chi_{lf}(10^{-8}m^3/kg)$
b
$\chi$ pedo
$\chi_0$
$(10^{-8}m^3/kg)$
Age(Ma)
c
Linear fit line
$R^2$=0.45 n=163
p (a) <0.01
Sr(ppm)
CaO*(%)
d
Linear fit line
$R^2$=0.12 n=163
Sr(ppm)
$CaCO_3$(%)
e
Benthic $\delta^{18}O$ (per mil)
$\chi_{pedo}$ $(10^{-8}m^3/kg)$

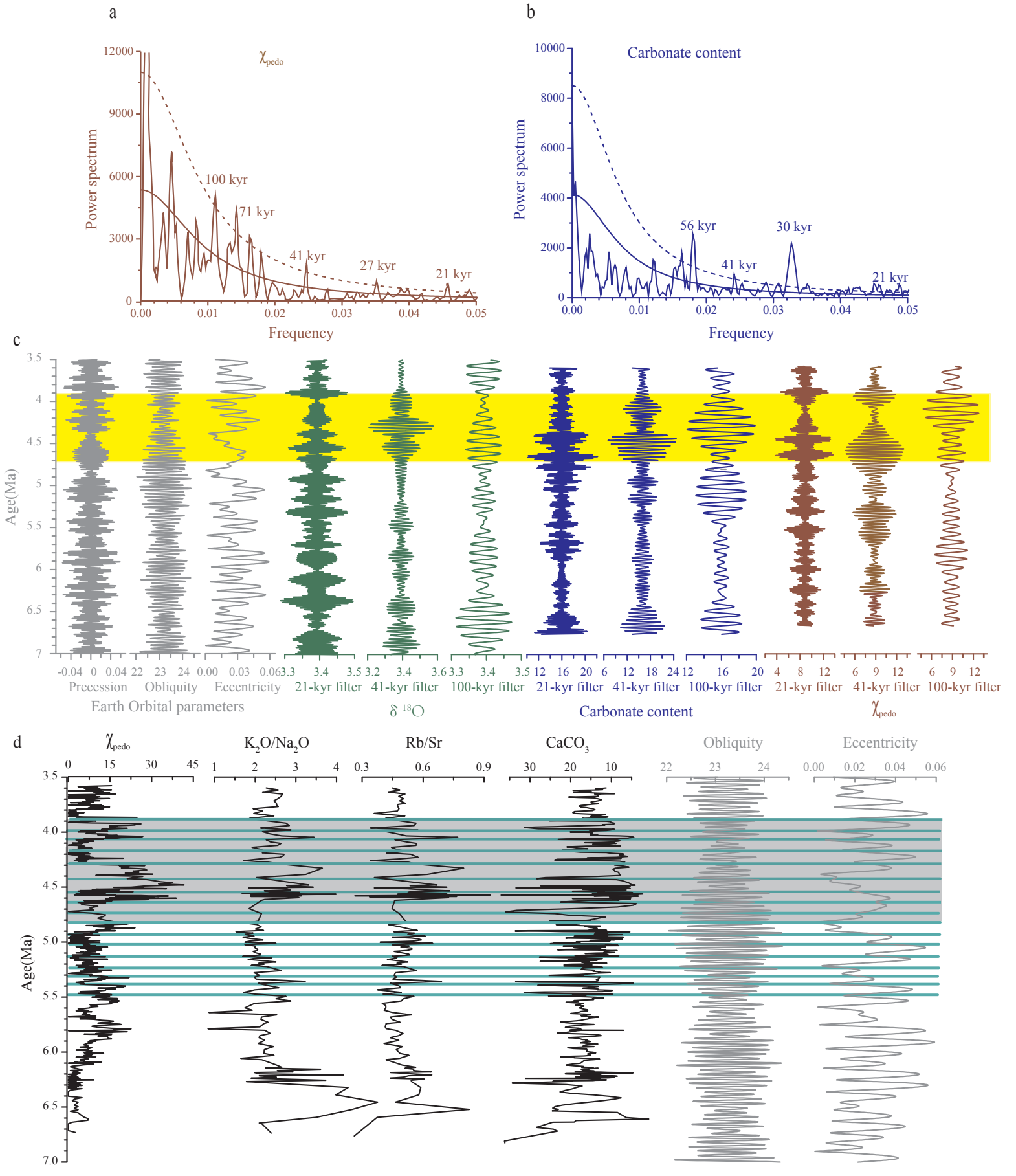


Fig. 5. Spectrum analysis results of the XSZ red clay section. (a) $\chi_{pedo}$ and (b) carbonate content. (c) Comparison of orbital parameters (eccentricity, obliquity and precession - Laskar et al., 2004) with filtered components of the carbonate content, $\chi_{pedo}$ and $\delta^{18}O$ records (Zachos et al., 2001) in the 18-24 kyr, 36-46 kyr, and 90-110 kyr bands. Yellow shading denotes increased amplitude of the filtered components of carbonate and χpedo within the three orbital bands. (d) Carbonate, weathering and pedogenic indicators linked to eccentricity and obliquity orbital variations during 4.7–3.9 Ma.

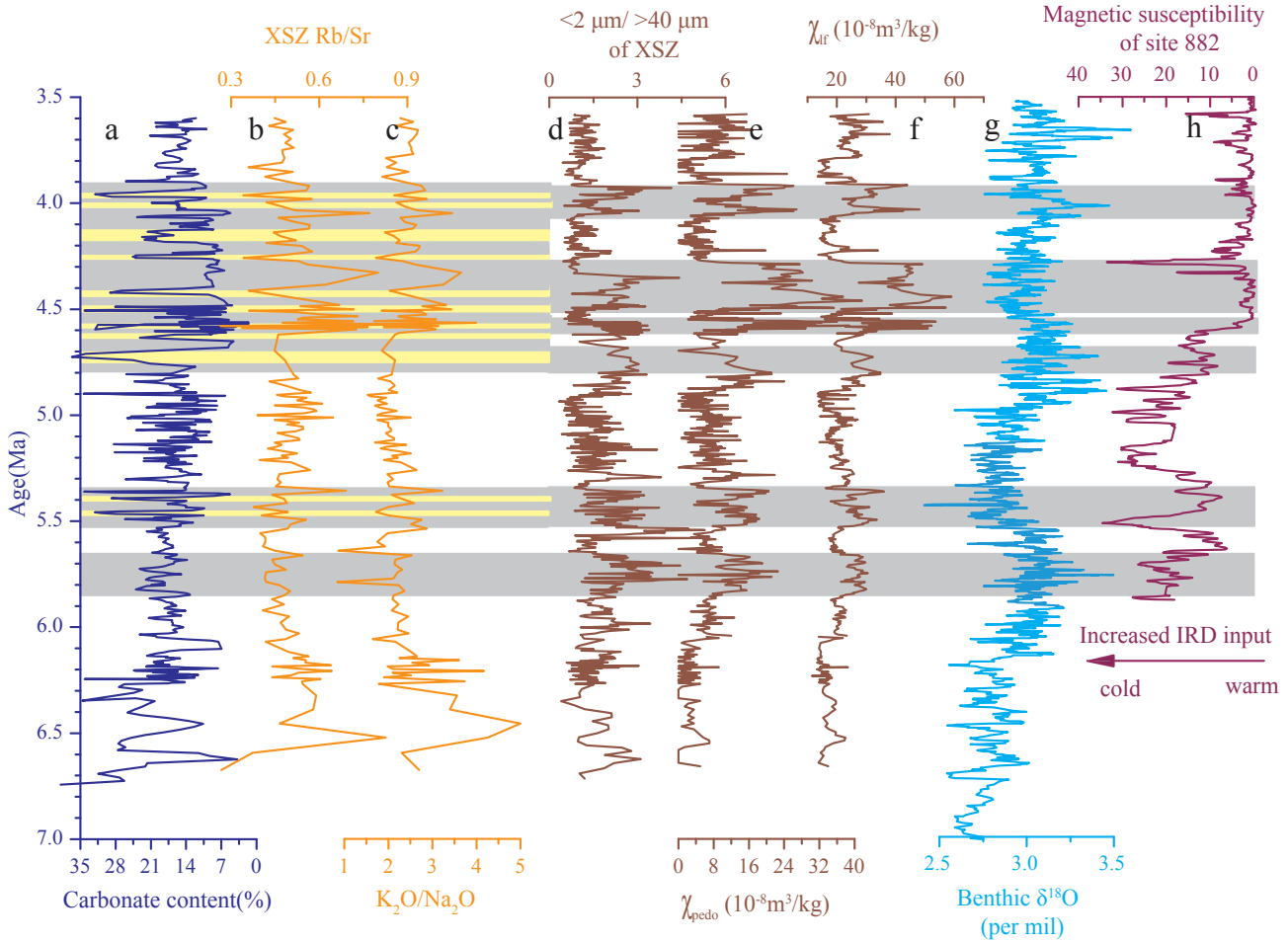
XSZ Rb/Sr
0.3
0.6
0.9
<2 μm/ >40 μm
of XSZ
0
3
6
χlf (10-8m3/kg)
20
40
60
Magnetic susceptibility
of site 882
40
30
20
10
0
a
b
c
d
e
f
g
h
Age(Ma)
3.5
4.0
4.5
5.0
5.5
6.0
6.5
7.0
Increased IRD input
cold
warm
35
28
21
14
7
0
Carbonate content(%)
1
2
3
4
5
K2O/Na2O
0
8
16
24
32
40
χpedo (10-8m3/kg)
2.5
3.0
3.5
Benthic δ18O
(per mil)

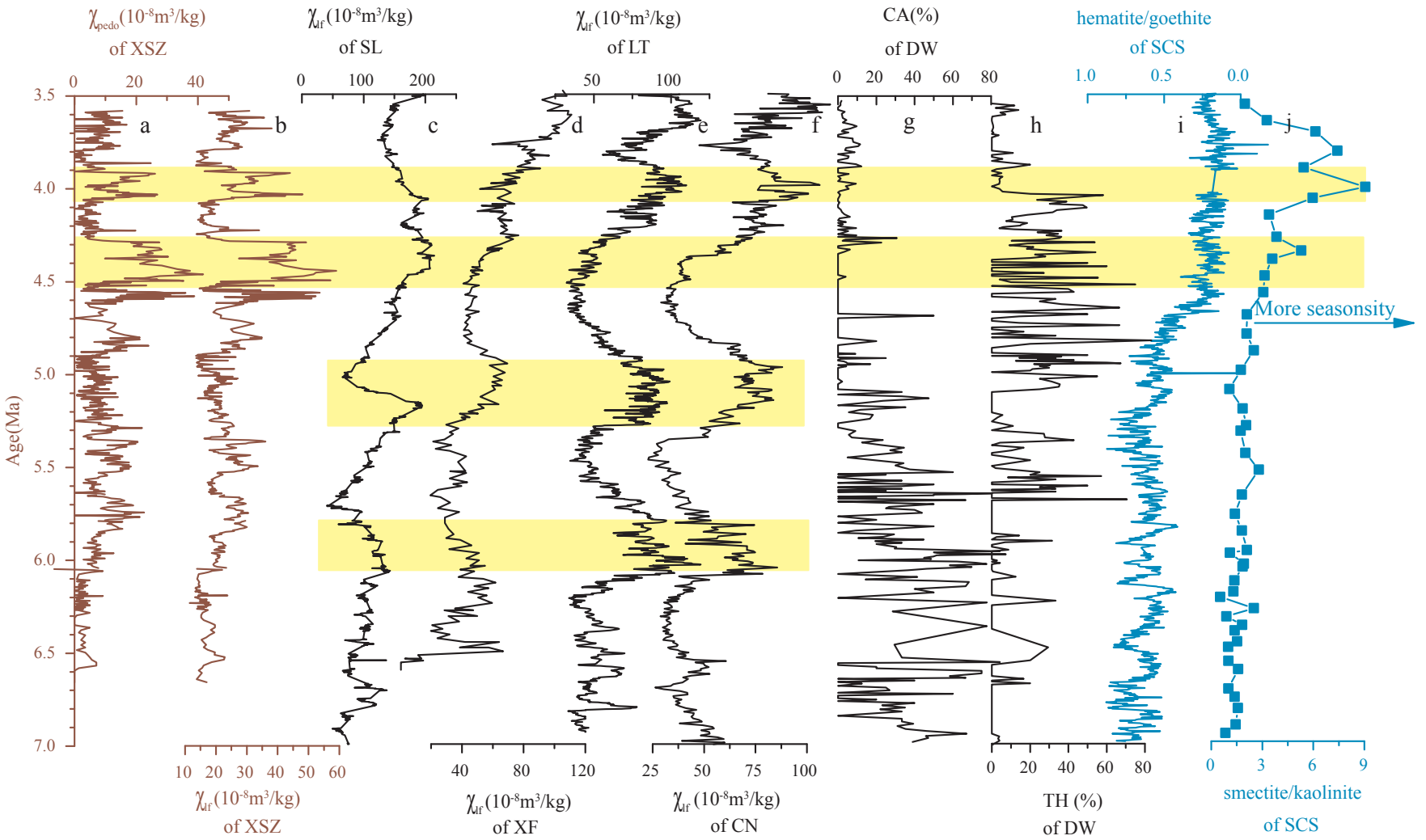


Fig. 7. Comparison of late Miocene-Pliocene paleoclimatic records from Asia. (a-b) χpedo and χlf from the XSZ section. (c-f) χlf record from Shilou (Ao et al., 2016), Xifeng (Guo et al., 2001), Lingtai (Sun et al., 2010) and Chaona (Song et al., 2007). (g-h) Percentages of cold-aridiphilous (CA) mollusks and thermo-humidiphilous (TH) mollusks from Dongwan (Li et al., 2008), (i) hematite/goethite ratio from sediments of the South China Sea (Clift, 2006), (j) smectite/kaolinite ratio from the South China Sea (Wan et al., 2010; Clift et al., 2014).

Table. 1. Average values and coefficients of variation of the geophysical and geochemical data for the XSZ section

| | | $CaCO_3$(%) | CaO(%) | $K_2O$(%) | $Na_2O$(%) | Sr(ppm) | Rb(ppm) |
|---|---|---|---|---|---|---|---|
| 3.9-3.6 Ma | Average | 15.5 | 12.8 | 3.0 | 1.25 | 228.1 | 106.6 |
| | CV | 16.0 | 12.5 | 10.8 | 9.3 | 5.8 | 4.6 |
| 4.7-3.9 Ma | Average | 13.3 | 11.2 | 3.1 | 1.21 | 210.4 | 111.0 |
| | CV | 53.6 | 45.3 | 13.8 | 10.5 | 14.0 | 12.1 |
| 6.7-4.7 Ma | Average | 17.1 | 11.2 | 2.6 | 1.22 | 211.7 | 103.9 |
| | CV | 28.2 | 31.7 | 10.3 | 20.9 | 9.9 | 10.8 |
| | | $\chi_{hf}$ | $\chi_{lf}$ | $\chi_{fd}$ | $\chi_{pedo}$ | Rb/Sr | $K_2O/Na_2O$ |
| 3.9-3.6 Ma | Average | 21.9 | 22.9 | 0.95 | 8.7 | 0.47 | 2.36 |
| | CV | 20.6 | 21.3 | 67.0 | 67.0 | 8.7 | 11.1 |
| 4.7-3.9 Ma | Average | 27.4 | 29 | 1.6 | 14.5 | 0.55 | 2.58 |
| | CV | 36.2 | 37.8 | 78.9 | 78.9 | 25.0 | 20.9 |
| 6.7-4.7 Ma | Average | 19.4 | 20.3 | 1.0 | 9.1 | 0.49 | 2.21 |
| | CV | 21.0 | 22.4 | 72.8 | 72.8 | 15.8 | 25.1 |

Table. 2. Correlation coefficients for geochemical data for the XSZ section

| Pearson correlation | CaO | $CaCO_3$ | $K_2O$ |
|---|---|---|---|
| CaO | 1 | 0.51 | -0.67 |
| $Na_2O$ | -0.06 | -0.10 | -0.38 |
| $K_2O$ | -0.67 | -0.47 | 1 |
| Rb | -0.20 | -0.36 | 0.12 |
| Sr | 0.24 | 0.34 | -0.29 |
| $CaCO_3$ | 0.51 | 1 | -0.47 |

Table. 3. Results of a significance test for the correlations between CaO*, $CaCO_3$ and Sr

| Pearson correlation | CaO* | $CaCO_3$ |
|---|---|---|
| Sr | 0.67** | 0.34 |
| sig.(2-tailed) | 0.000 | 0.063 |
| n | 163 | 163 |

**Correlation is significant at the 0.01 level